Peer-reviewed version available at J. Mar. Sci. Eng. 2019, 7, 158; doi:10.3390/jmse7050158

Article

Stochastic modeling of forces on jacket-type offshore structures colonized by marine growth

Hamed Ameryoun [1*], Franck Schoefs [2], Laurent Barillé [3], Yoann Thomas [4]

[1] Université de Nantes, IXEAD/CAPACITES Society, Nantes, France; hamed.ameryoun@capacites.fr
[2] Université de Nantes, Research Institute in Civil Engineering and Mechanics - GeM - UMR CNRS 6183, Sea and Littoral research Institute, IUML - FR CNRS 3473Nantes, France; franck.schoefs@univ-nantes.fr
[3] Université de Nantes, Mer Molécules Santé EA 2160, Sea and Littoral research Institute, IUML - FR CNRS 3473Nantes, France; laurent.barille@univ-nantes.fr; yoann.thomas@ird.fr
[4] IRD LEMAR - IUEM, rue Dumont d'Urville 29280 Plouzané, France +33 2 98 49 86 43
* Correspondence: franck.schoefs@univ-nantes.fr

Received: date; Accepted: date; Published: date

Abstract: The present paper deals with the stochastic modeling of bio-colonization for the computation of stochastic hydrodynamic loading on jacket-type offshore structures. It relies on a multidisciplinary study gathering biological and physical research fields that accounts of uncertainties at all the levels. Indeed, bio-colonization of offshore structures is a complex phenomenon with two major but distinct domains (i) marine biology whose processes are modeled with biomathematics methods and (ii) hydrodynamic processes. This paper aims to connect these two domains. It proposes a stochastic model for the marine organism's growth and then continues with transfers for assessment of drag coefficient and forces probability density functions that accounts for marine growth evolution. A case study relies on the characteristics (growth and shape) of the blue mussel (Mytilus edulis) in northeastern Atlantic.

Keywords: marine growth; biofouling; wave loading; stochastic modeling; reliability; jacket structures

1. Introduction

Actual challenges for requalification of existing offshore structures through the reassessment process emphasizes the importance of updating information about the state of structural safety. One of the most important phases during the design or re-assessment level is a re-evaluation of environmental loads and updating data concerning the state of biocolonization, structural damage, and corrosion. The random nature of biofouling and the uncertainty inherent to biological processes make modeling of environmental loading complicated. Biofouling is a complex phenomenon involving a diversity of marine species, which constitute communities whose dynamic is driven by physical and biological processes. It has many negative impacts on offshore structures such as loading excess, structures occlusion, increase in drag coefficient, and corrosion. Therefore, it represents a challenge for engineers with respect to design and maintenance programs. Several standardized methods of inspections and *in-situ* measurements of the marine growth have been developed to obtain relevant information about species composition, percent cover, weight, thickness and roughness allowing the determination of structural design, cleaning and maintenance strategies. Biocolonization processes show spatial and temporal variations related to several environmental factors (water temperature, hydrodynamics, turbidity, distance from the shore, bottom characteristics) acting at regional and local scales. However, the results are often more qualitative than quantitative and suffer from a lack of consistent modeling for structural engineers except when a big database is available. Cost-effective, safety management of offshore structures involves allocating the optimal amount of resources to periodical inspections and maintenance activities in order to control risks (expected life of the structure). The present paper considers the

biocolonization as a cumulative deterioration process and defines two phases for it: an initiation phase and a propagation phase. It reviews meta-models, describes database construction which consists of the influencing factors. It proposes a stochastic modeling of biofouling based on non-stationary, state-dependent Gamma process for the blue mussel *Mytilus edulis*. The developed Gamma process provides individual shell length time series for blue mussels in the first year of colonization. The results reveal that the method can capture the distribution and especially extreme values of observed shell length. Thereafter, the study focuses on the drag term of the Morison's equation. It reviews a response surface method to model the drag force as well as the effect of physical characteristics of structural members such as surface roughness (k) and average thickness of marine growth (Th). Moreover, the drag force exerted by extreme waves for colonized structural members during the typical macro-colonization years is determined. The probabilistic macro-colonization, shell length time-series considering the occurrence probability of typical macro-colonization years are provided. The evolution of the drag coefficient with regard to the probabilistic shell length time series is evaluated and the results are discussed.

The growth of marine organisms on offshore structures has long been a significant issue for the oil and gas industry ([1]-[2]). In the 70's and 80's, studies focused on the effect of biofouling on hydrodynamic forces acting on offshore structures. Numerous experimental studies were carried out with different types of marine growth, cylinder diameter, and hydrodynamic conditions to provide a better understanding of their interactions with hydrodynamic forces and to highlight the key relationships. Despite the great variability due to the complexity and instabilities of the flow regime around structures, abacus were built and are still recommended by offshore standards such as API [3] and DNV [4]. Only a few studies considered the global modeling of the loading in a probabilistic context ([5]; [6]) and none of them consider the modeling of the organismal growth itself. In fact, there are few available databases containing on-site measurements with time ([7]; [8]). This paper proposes a modeling of characteristics of the external marine growth layer consistent with structural engineering needs. As the first year is crucial for future colonization patterns, we focused here on the building of the first layer of biofouling by a macro-fouler. The blue mussel *Mytilus edulis* was considered for the modeling, as it is an ubiquist bio-fouler in European waters ([9]; [10]).

A biological model based on the Dynamic Energy Budget (DEB) theory ([11]; [12]) was used to simulate the variations of individual mussel shell size depending on environmental data. A case-study site was chosen offshore the Loire Estuary (France) corresponding to a future offshore wind farm site. In order to model the colonization during the first year, two main phases of bio-colonization were considered: 1) an initiation phase without any macro-fouling on the structure and 2) a propagation phase or macro-colonization phase, corresponding to the growth of mussels. The key influencing factors affecting these two stages were hydrological data (water temperature and chlorophyll-a concentration, as proxy of mussel food). Mussel growth was used to derive two geometrical characteristics describing marine growth: average thickness (Th) and surface roughness (k). A case study is considered in view to illustrate the role of these biofouling geometrical variables on the computation of hydrodynamic forces (drag force) for colonized structures and study the effect of bio-colonization on the drag force.

The next step was to shift from this deterministic approach to a full probabilistic context. A non-stationary state-dependent Gamma process ([13]; [14]) was therefore developed to model the mussel colonization of the first year. As far as the authors know, it is the first time that bio-colonization is considered as a consecutive stochastic jumps governed by a gamma process. In order to obtain geometrical characteristics of colonized surfaces, state-dependent non-stationary Gamma process generated individual shell length growths trajectories for blue mussels in the first colonization year with a probabilistic approach. The parameters of the state-dependent non-stationary Gamma process were estimated after identification of key environmental factors. Modeling individual shell growth as a cumulative degradation phenomenon during the colonization process was used to compute the biofouling geometrical variables (Th and k). Finally,

the effect of blue mussel colonization on the evolution of drag coefficient and loading exerted by the extreme waves was analyzed. It should be noted that the added mass and inertia forces are beyond the scope of this paper.

The objective of this work is to propose a meta-model, which combines different disciplinary approaches accounting for several types of uncertainty and variability amongst: (a) the temporal variability of the main influencing environmental factors; (b) the biological uncertainty of the individual's growth; (c) the uncertainty due to the modeling of geometrical parameters of structural components caused by biofouling and needed for structural computations; (d) the uncertainty of wave characteristics to compute the loading on structural components. To propagate the uncertainty, a physical matrix response surface was used in view to provide a probabilistic model of the environmental loading on jacket type offshore structures based on Schoefs & Boukinda (2010) [1]. This method was applied for quasi-static calculations of wave forces in presence of marine growth.

2. Materials and Methods

2.1 Requirements for a meta-model

To develop the macro-colonization model for structural computation several properties should be considered: the main trends of growth with time should be captured using time step compatible with sensitivity to input parameters; it should be sensitive to the environmental parameters that govern the ecophysiology of the biofouling: temperature and food availability; it should provide intermediate parameters (shell size) from which required outputs can be easily computed (roughness and thickness) to perform a reliability analysis (stochastic processes); it should be versatile to modify the trends depending on site specificity. The next sections detail the way these requirements have been taken into account in this work.

2.2 Description of bio-colonization temporal dynamic

Bio-colonization is a complex process depending on biotic and abiotic variables with many interactions ([15]; [16]). Actually, it would be unrealistic to envisage a complete model involving a multilayer of various marine organisms that have complex interactions for survival, growth, and reproduction. We propose here a model that accounts for the temporal variability of the main influencing factors in a simplified but realistic case. It focuses on the growth of a single species, the blue mussel Mytilus edulis.

The bio-colonization process depends on two early stages: (1) the reproduction of adults, which spawn in the water column and produce larvae that will become part of the plankton transported by currents; (2) larval survival and development in the water column. The bio-colonization itself starts with the larval settlement on a structure (micro-colonization) and corresponds mainly to the macro-colonization step i.e. growth of individuals up to the adult state. It is important to estimate the spawning date(s) and to assess the conditions allowing larval survival. This is a prerequisite before modeling macro-colonization. Consequently, the model needs to take into account (1) an initiation phase (no macro-organism present on the structures) with no significant effect on structural reliability and (2) propagation phase corresponding to the growth of macro-organisms (Figure 1). With these two phases, an analogy can be made with the dynamic of degradation processes like corrosion of steel rebars in reinforced concrete [17]. In this study, we considered that the larval settlement corresponds to the beginning of the propagation phase.

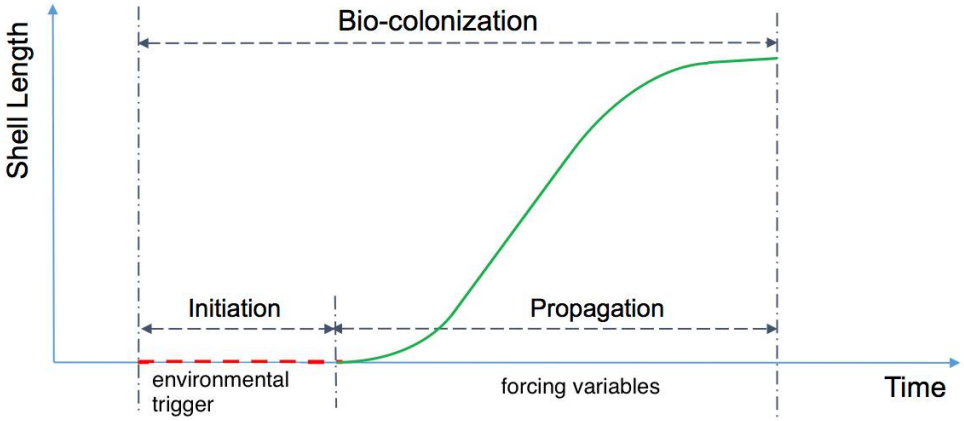

Figure 1. Schematic diagram of bio-colonization phases and their influencing parameters.

The model should be able to capture the initiation phase and then simulate a propagation phase (macro-colonization). The latter allows for obtaining the individual size and accordingly the physical characteristics of the colonized surface needed for the hydrodynamic calculations [6]. The initiation phase includes spawning date, larval survival, development, and settlement. We considered that this phase was mainly driven by temperature while the propagation phase (macro-colonization) corresponding to the juvenile growth was driven by both, the temperature and the concentration of chlorophyll-a, proxy of the food available in the water column for mussels. These drivers are related to the bivalve ecophysiology, which is detailed in the following paragraph.

2.3 *Description of bio-colonization temporal dynamic*

The blue mussel Mytilus edulis was chosen to develop a simplified (single organism colonization) but realistic bio-colonization model for the North-Atlantic coasts. M. edulis is an ubiquitous and abundant species in the coastal waters of the North and Mid-Atlantic Regions [18], and has been reported as a main macro-colonizer of offshore structures ([19]; [20]). When found as a dominant hard fouler, it has an influence on the composition of external layer of marine growth [15]. It is a suspension-feeding bivalve that attaches to substrata by byssal threads and is traditionally cultivated on ropes or wooden poles on the Western Atlantic coasts [21]. M. edulis is eurythermal (adaptable to a wide range of temperatures) and under the latitude of our case-study site, is well acclimated to a 5 to 20°C temperature range [22]. It is very common in the intertidal area forming beds on rocky and hard substrates but can be found in subtidal environment down to -10 m. Mussels feed on suspended particulate matter and their main food resource is phytoplankton cells ([23]-[25]). Phytoplankton is also considered as the dominant food source for all life stages of M. edulis since larvae also rely on phytoplankton for their development. The concentration of chlorophyll-a is a widely used proxy of phytoplankton biomass, and this variable was used in this study to assess the food available for the mussel's growth. For more details on M. edulis morphology, physiology and ecology, the reader is referred to Gosling (2003) [21].

2.4 *Initiation phase and propagation phases*

The spawning date, larval survival, and development are the most important stages for the initiation phase modeling. Blue mussels, like the majority of shallow water bivalves, produce large numbers of pelagic planktotrophic larvae that spend several weeks in the surface waters [25]. M. edulis sexes are separated and gametes are shed into the water where fecundation occurs. At the latitude of the study site, mussels can spawn up to three times a year from April to September successively, depending on environmental factors. In bivalves, an essential condition related to spawning is a thermic threshold corresponding to a minimum water temperature [26]. Indeed, the temperature is the strongest exogenous factor controlling M. edulis reproduction [21]. In this work, we considered only the spring period when the mussel producers submerge ropes to collect planktonic larvae. In Pertuis Breton, which is the closest area to our study site, Barillé-Boyer (1996)

[22] found a threshold of 10.5 °C and it has been considered that spawning was not triggered below this temperature. Above this temperature, the spawning dates are not modeled but forced with observed datasets [24]. In this study, observations from mussel producers are used. A 30-day interval between two spawning was adopted in relation to the mussel gametogenesis dynamic. This delay is linked to the time necessary to reconstitute reproductive tissues [22]. Other exogenous factors such as storms, shock, rain, etc., which can randomly trigger bivalve's spawning, were not considered. The second important step following spawning is the larval survival and development. For mussels, Bayne (1965) [27] observed that M. edulis larvae could reach its development within 20 to 40 days, depending on the temperature. A slower (S) larval growth and metamorphosis can take 40 days if spawning happened in early spring with the water temperature of around 10°C, while a faster (F) larval development of around 20 days is possible at a higher temperature of 14°C [22]. Therefore, it was considered that if during the next 20 days after spawning water temperature was > 14°C, larvae survival and development was completed in 20 days, otherwise in 40 days. For each year in our database, the spawning occurrence times and initiation phase typologies are determined by post-processing the temperature time-series.

As mentioned before geometrical parameters (thickness and roughness) are required for load computation. They depend on geometrical specifications (shape) of organisms colonizing the structure. In this study, these parameters are linked to the shell length of blue mussel individuals. Shell growth of blue mussel has an asymmetric sigmoid shape curve ([28]; [29]). The growth rate of blue mussel individuals is, therefore, neither monotonic nor stationary, and the growth curve can be described by the acceleration and deceleration phases (Figure A1, in appendix A). No clear relationship between the individual shell growth and the water temperature has been observed, while the concentration of chlorophyll-a appeared to be the main driver. This observation is consistent with several studies showing that the food supply was the most important variable explaining mussel growth (([30]-[32]).

2.5 Database post-treatment, Virtual database, and aggregation of influencing factors

2.5.1 Environmental data at the case-study site

In order to model the initiation and propagation phases, water temperature and chlorophyll-a (*Chl. a*) concentrations were obtained for the site of Le Croisic (47°17'33" N, 2°31'15" W) western Atlantic coast of France. This location was chosen for its proximity to the future offshore wind farm site of Banc de Guérande (47°19'41" N, 2°25'46" W). Data were collected by the French Phytoplankton Monitoring Network (REPHY) implemented and managed by the French Research Institute for the Exploitation of the Sea (Ifremer). Bimonthly samples were collected at sub-surface depth (between 0 and 1 m) during high tides between 1996 and 2012 (Figure 2). Chlorophyll a display higher concentration between March to June corresponding to the spring phytoplanktonic bloom characteristic of northern hemisphere temperate waters. In 2004, a single spring peak was observed, while in 1996, three peaks of lower concentrations were detected. It should be noted that the water temperature cannot change abruptly in a short time. For an overview of the REPHY network, the reader is directed to Hernández Fariñas (2015) [33] and Hernández Fariñas et al., (2013) [34].

Preprints (www.preprints.org) | NOT PEER-REVIEWED | Posted: 16 April 2019 doi:10.20944/preprints201904.0183.v1

Peer-reviewed version available at J. Mar. Sci. Eng. 2019, 7, 158; doi:10.3390/jmse7050158

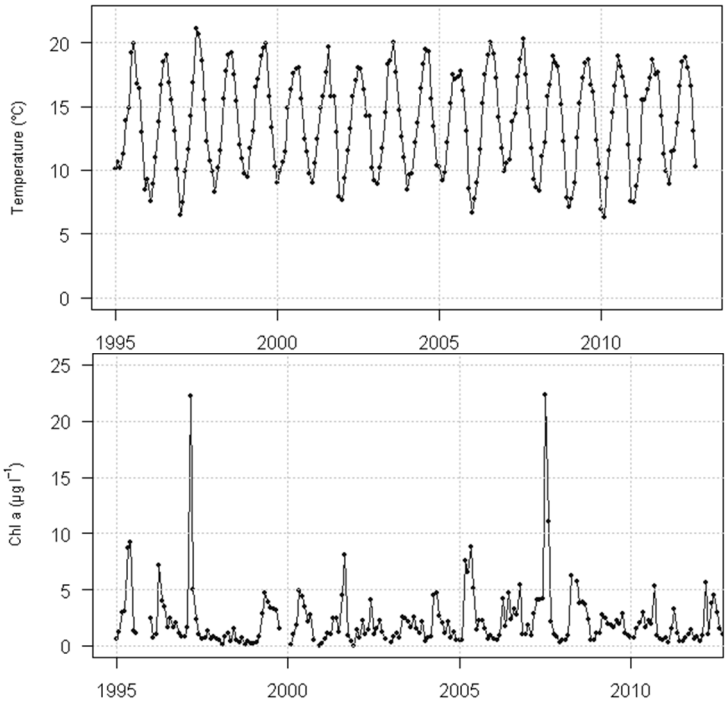

Figure 2. Inter-annual variations (1996 - 2012) of water temperature (°C), and chlorophyll-a (chl a, µg L-1) at Le Croisic sampling station (Loire-Atlantique, France). Data from Ifremer/Quadrige/Rephy©.

In order to model bio-colonization and to standardize the time intervals of data acquisition, each month has been divided into three 10-days periods. The database used hereafter has been therefore constructed from periodic observations at established time intervals τ equal to 10 days. It should be noted that the water temperature could not change abruptly in each 10-days period. The number of the database time-series [Year Time-step] is defined by N, representing the number of years for which the database base has been prepared, and t, which represents the number of observations each year depending on the data acquisition time intervals τ; in our case N=17, t=37 and τ=10. The long-term time-variant modeling of input factors being out of the scope of this work, we assumed that N is statistically sufficient for computing the frequency of each macro-colonization scenario. Therefore, the database has been constituted from the regular measurements of water temperature (T) and *Chl. a* (C), and can be denoted as:

$$\left\{\left(T_{t,\tau}^{i}, C_{t,\tau}^{i}\right); t \geq 0, \mathrm{i} \in [\![1, \mathrm{N}]\!]\right\} \quad (1)$$

Hereafter, $T^{i}_{t,\tau}$, is used for the initiation phase determination and $C^{i}_{t,\tau}$ for the modeling of the propagation phase. Four types of larval development combining the slow (S) and fast (F) growth possibilities are presented in the Table 1 for the three initiation times (corresponding to the three spawning periods) obtained from the database considering key factors and thresholds described in the previous section. The first larval development is always slow due to water temperature below 14°C during early spring, and the third one can be slow only if the second one is also slow (because the water temperature cannot fluctuate abruptly). These results come from the natural seasonal variations of temperature during one year. These frequencies will be considered as discrete probabilities for the modeling. At the end of this larval growth period, we considered that larvae settled on the structures, and that was the start of the propagation phase (macro-colonization) described in Table 1 for the 17 annual chronicles.

Table 1. Inter-annual development types for three main spawning events (S: slow initiation phase, F: fast initiation phase)

Development type	Occurrence	Probability
SSS	2	0.12
SSF	10	0.59
SFS	0	0.00
SFF	5	0.29

Table 2 shows the date of start of macro-colonization, expressed in 10-days periods (1 = first 10 days of January), for three main spawning events of blue mussel between March and June. Occurrence and probability were calculated from the 17-year time-series of temperature data at the study site. Calculations revealed that macro-colonization starting date spanned from the 11th to the 20th 10-days period. The most probable macro-colonization inception times for the three spawning events corresponded to the combination of 10-days periods of 12-15-16 and 13-16-17 with 18% probability. The first macro-colonization inception occurred between the 11th and the 16th 10-days periods with the highest probability of 29% for 11th period and the lowest probability of 6% for the 16th period. The second macro-colonization inception occurred between the 14th and 17th periods with the lowest probability of 12% for the latter. The third macro-colonization inception occurred between the 17th and the 20th periods with the highest probability of 35% for the 17th period and the lowest (6%) for the 20st.

Table 2. Date of start of macro-colonization, expressed in 10-days periods, for three main spawning events of blue mussel.

Start of macro-colonization			Occurrence	Probability
11	14	15	2	0.12
11	14	17	2	0.12
11	15	16	1	0.06
12	15	16	1	0.18
13	14	17	1	0.06
13	16	17	3	0.18
14	15	18	1	0.06
14	17	18	1	0.06
15	16	19	2	0.12

2.5.2 Environmental data at the case-study site

There was no observation available for blue mussel shell lengths close to our study site and more generally, no database for the annual growth of mussels during the considered 17-year period. To fill this gap, we applied a bioenergetics growth model to simulate the individual shell length using environmental time-series data available at the study site. Different bioenergetics models have been developed to model the growth of bivalves depending on the environmental conditions, and among them, Dynamic Energy Budget (DEB) models [11] have been successfully applied to several bivalve species ([24]; [35]-[38]). DEB models do not use empirical allometric relationships, but simply state that feeding is proportional to surface area, whereas maintenance is scaled according to structural body volume [11]. DEB theory proposes a generic energy budget approach that assumes

Preprints (www.preprints.org) | NOT PEER-REVIEWED | Posted: 16 April 2019 doi:10.20944/preprints201904.0183.v1

Peer-reviewed version available at J. Mar. Sci. Eng. 2019, 7, 158; doi:10.3390/jmse7050158

common physiological processes among species and life stages via a set of parameters, the only difference among species lying in the values of those parameters.

In this study, we used the DEB model developed by Thomas et al. (2011) [31] to simulate the growth of Mytilus edulis in the Mont Saint-Michel Bay. A single parameter, the half-saturation coefficient of the food ingestion function term (XK) had to be adjusted to local hydrologic and trophic conditions. For our study, the half-saturation coefficient was calibrated at 2.9 $\mu g.L^{-1}$ from growth data by Garen et al. (2004). Simulations started for 1 mm individuals (0.02 g of Dry Flesh Mass - DFM), a biometry corresponding to post-settled organisms. Results of the calibration are presented in Figure A2 in Appendix A. A good level of agreement between observations and simulations was obtained for shell length and dry flesh mass, a biological variable often used in bioenergetics models to assess the consistency of the simulations.

The model was then used to obtain individual growth trajectories with the 17-year time-series of *Chl. a* concentration measured at Le Croisic (Loire-Atlantique, France). Three starting dates were chosen, corresponding to the three spawning events and related macro-colonization starting dates (Figure 3).

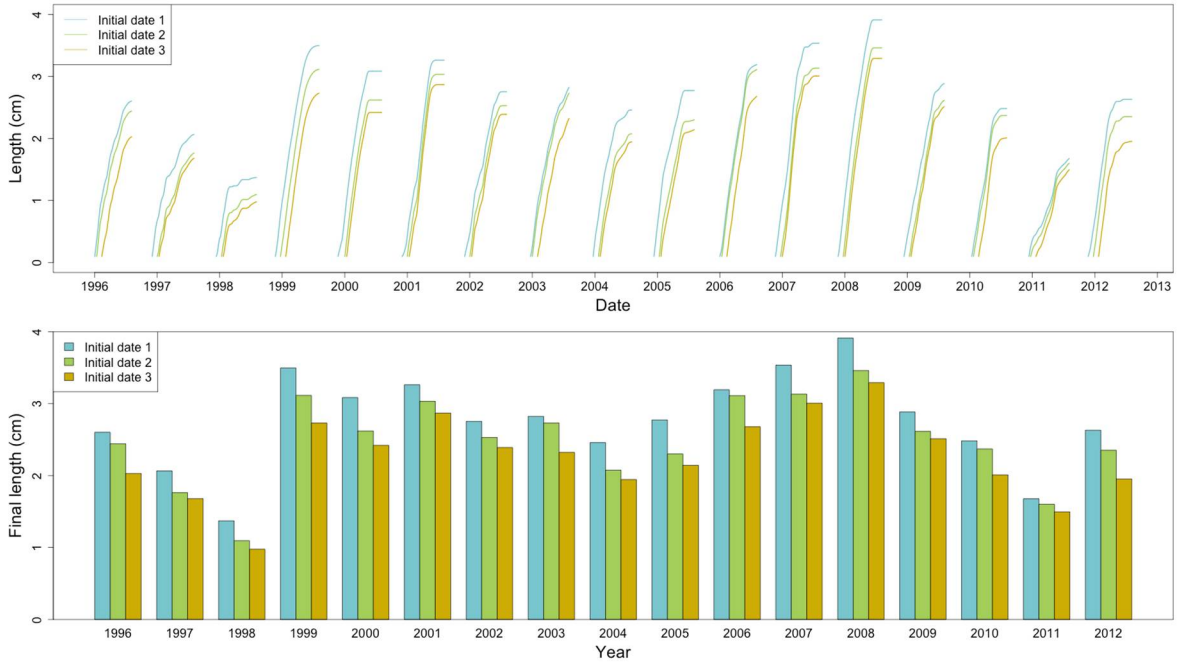

Figure 3. (a) Individual annual shell length trajectories simulated by a mussel DEB model and (b) corresponding final length.

2.6 *The relation between environmental factors, growth, and the start of macro-colonization*

The Gamma process simulates increments for each time interval of τ which correspond here to variations in mussel shell length ($\Delta S_{t,\tau}$). The parameterization of the function can integrate the environmental variables. Temperature is a variable of the DEB model, but *Chl. a* concentration is the main driver of growth. It was therefore decided to parameterize the Gamma process only with *Chl. a*. However, due to potential coupled effects between temperature and *Chl. a*, we analyzed the correlation between temperature and growth over the time-series. From ΔS obtained from DEB simulations, the scatter diagram of ΔS vs. temperature showed that there was no significant correlation between these two variables with a Pearson correlation coefficient ϱ=0.21 (Figure 4). On the contrary, there was a structured relationship between growth and *Chl. a* (Figure 5). It can be noted that uncertainty increases when *Chl. a* increases. Moreover, there is a ΔS plateau showing that the capability of an individual to grow is limited whatever the additional food supply: a

concentration higher than 8 µg.L^{-1} does not lead to larger ΔS. This is due to a well-described physiological phenomenon of maximum somatic growth in bivalves ([39]; [40]).

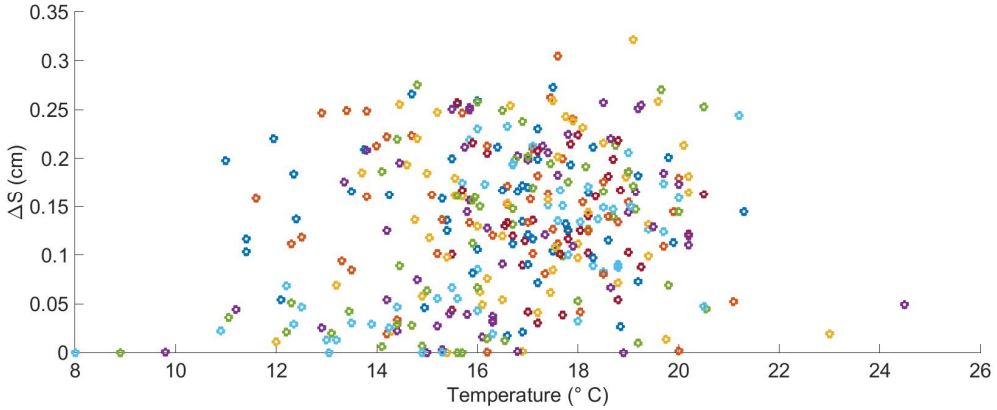

Figure 4. Scatter diagram of the variations of mussel shell length (ΔS) vs. temperature for 10 days periods during the 17-year time series (each color represents a year of the 1996-2012 time-series).

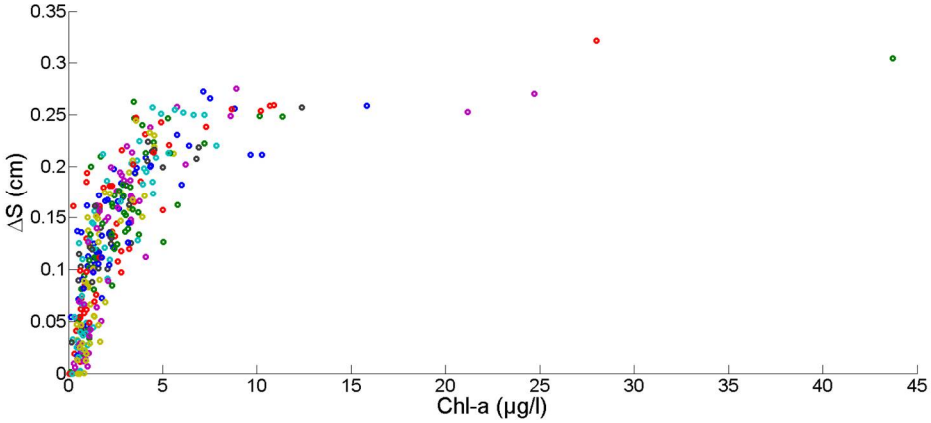

Figure 5. Scatter diagram of the variations of mussel shell length (ΔS) vs. Chlorophyll a for 10 days periods during the 17-year time series (each color represents a year of the 1996-2012 time-series).

The relationship between the start of macro-colonization and the concentration of *Chl. a* is presented in Figure A3 in Appendix A. There is no significant correlation between these two variables with a Pearson correlation coefficient ϱ= -0.02. This property is of first importance, as it will govern the simulation strategy. Simulation of inception times (start of macro-colonization) requires temperature time-series only and the modeling of mussel growth will be carried out independently using *Chl. a* time-series.

2.7 Chlorophyll data aggregation for growth computation

In order to improve the biological consistency of our simulations, we tested the possibility to link the individual growth of blue mussels to *Chl. a* concentration aggregated over a time-step instead of using instantaneous values. The integrated value of *Chl. a* was simply defined as:

$$C_{(T_{(i)}:T_{(i+n)})} = \frac{1}{n}\int_{T_{(i)}}^{T_{(i+n)}} Chl(t)dt,\ \mathrm{i}=1:36-\mathrm{n} \qquad (2)$$

where *C(t)* is the aggregated *Chl. a*; $T_{(i)}$, is a10-days period and *Chl(t)*, is the linear equation of *Chl. a* obtained from linear interpolation between adjacent measured values for a colonization

period, and n is the number of 10-day time intervals after (i), in which the data aggregation is performed. The best correlation between ΔS and *Chl. a* have been obtained for a monthly aggregation (3-time intervals, n=2 in (2)). This time-step preserved the spring bloom typical of the seasonal dynamic of phytoplankton at the study site latitude.

In order to identify the non-linear relationship between growth and *Chl. a*, the non-linear regression (3) has been fitted (Figure 6):

$$\Delta S = \frac{0.235}{1+6.94e^{-1.005(Chl.-a)}} \quad (3)$$

The ratio of ($d\Delta S$ / $dChl.\ a$) ≤2% has been chosen as a criterion for stabilization based on slope variations; this ratio is consistent with the accuracy of the DEB model. A concentration of *Chl. a* of 8 µg.L^{-1} was identified as the threshold beyond which ΔS remained constant at 0.235 cm/ time interval. The *Chl. a* time-series was then truncated with the mentioned threshold to significantly improve the convergence of the Gamma process parameterization, without an important degradation of the database. Note that this threshold depends on the metabolism of the organism and is, therefore, species-specific.

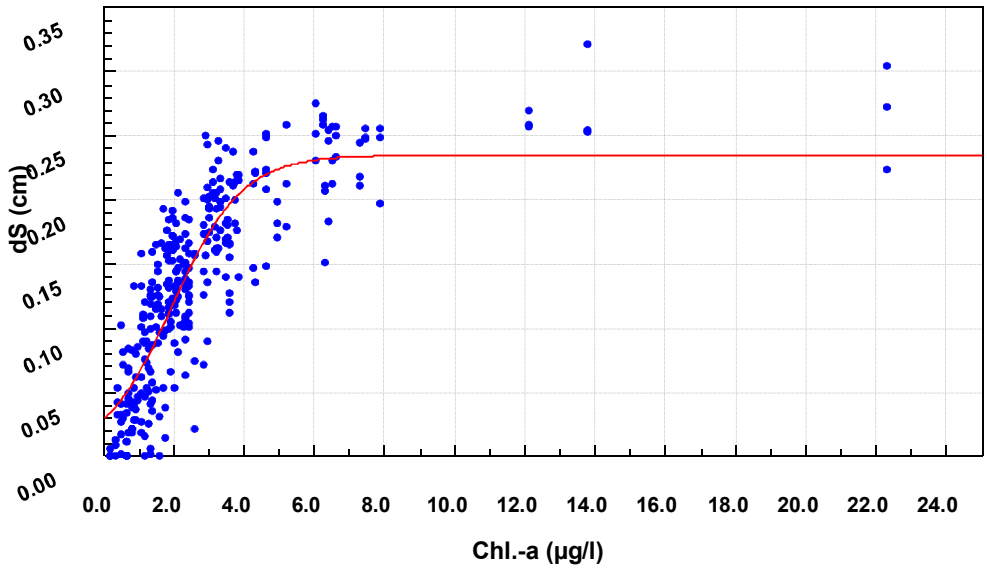

Figure 6. Identification of the chl. a threshold beyond which growth saturation is observed.

2.8 Non-stationary modeling of shell growth through stochastic Gamma process

2.8.1 Growth approximation through gamma processes meta-models

Considering the aforementioned characteristics of the mussel's colonization and in order to model the temporal dynamic of structure deterioration, a stochastic approach based on Gamma processes has been selected [41]. Since the introduction of the Gamma process in reliability [42], it has been used commonly to model stochastic cumulative and uncertain deterioration phenomena for maintenance optimization of various industrial systems. Indeed, the Gamma process is an analytically tractable stochastic process accumulating over time in a sequence of positive increments. Recently, it has been widely used to model cumulative degradation processes such as corrosion, fatigue, crack growth, creep, degrading health, erosion, and wear in engineering systems and structures ([13]; [41]; [43]; [44]).

The Gamma process is a special case of a non-decreasing jump stochastic process that properly captures the temporal variability associated with the deterioration dynamic. This justified the choice of the non-stationary state-dependent Gamma process. The non-stationary Gamma process is a widely used mathematical model to describe degradation process whose growth rate at time t depends only on the current state of the parameters and not on the accumulated damage up to t [45]. The complete Gamma process function is defined by two parameters: a shape function α_S and a scale function β_S (4). We discredited time horizon into equal intervals of length τ=10 days. Then, the state-dependent non-stationary and bivariate Gamma process was represented as a series of state-stationary Gamma processes in each time interval. The rate of the deterioration process can thus be considered as the process resulting from the Gamma process variations from one time-interval to another. The deterioration increment in a given time interval $\Delta S_{t,\tau}$ has been considered a random variable with a shape function (α_S) dependent of the present deterioration state $S_{t,\tau}$ and a second variable, the state of chlorophyll-a concentration $C_{t,\tau}$. Thus, for each time step τ, we have:

$$\forall S_{t,\tau} > 0 :\ S_{t,\tau}, \Delta S_{t,\tau}, \tau :\ \Delta S(\tau; \mathrm{S}_t, C_t) \sim Gamma(\alpha_s(\mathrm{S}_t, C_t).\tau, \beta_S) \quad (4)$$

Where, $S_{t,\tau}$ is the shell length for each time interval of τ and α_S and β_S are the shape and scale functions of the Gamma process, respectively. To simplify the modeling of this process, it has been assumed that the scale function β_S was constant and Gamma process was only governed by the shape function [13].

2.8.2 Parameter estimation of the Gamma process (learning phase)

In order to simulate the growth of blue mussel submitted to fluctuations of *Chl. a* in each time interval τ, the parameters of the developed Gamma process have to be estimated. The deterioration increments have been calculated by the simple subtraction of consecutive individual shell lengths and the resulting database used for deterioration density estimation is denoted as:

$$\left\{\left(C^i_{t,\tau}, S^i_{t,\tau}, \Delta S^i_{t,\tau}\right); t \geq 0, \mathrm{i} \in [\![1, \mathrm{N}-1]\!]\right\} \quad (5)$$

Where N is the number of 10-day time periods (in this study N=17). In order to estimate the parameters of the Gamma process, the Expectation-Maximization (EM) method has been employed. The program starts by scanning the database and indexes the values of *C(t)* and *S(t)* time-series; then using the observed data, initial parameters are estimated and used to start an iterative EM algorithm. The Gamma process parameters have been estimated and determined as:

$$\Delta S(\tau; \mathrm{S}_t, C_t) \sim \Gamma(\alpha_S = (0.198 + 1.68\,\mathrm{C}_t) \times \exp(\frac{-(S_t - 0.44)^2}{6.512}),\ \beta_S = 0.039) \quad (6)$$

2.8.3 Parameter estimation of the Gamma process (learning phase)

Once the Gamma process has been estimated, the DEB data are not needed anymore and we can use the *Chl. a* database to predict the growth rate of mussels. The macro-colonization can be then simulated with the Gamma process function (6) and considering the *Chl. a* database for 10 typical macro-colonization years from the 17-year time-series. We considered this database to be representative of the dispersion and respecting the frequency of the main phenomena and their consequences of a richer database. Thus, each environmental input (*Chl. a* time-series *C(t)*) is considered with the same weight as growth uncertainty (biological process). The 5000 simulated growth curves obtained by the Gamma process and individual growth curves simulated with the DEB model are compared in Figure 7. Each growth curve is simulated from one realization of the Gamma process with Chl. a randomly sampled from the 17-year time-series database: uncertainties for *Chl a.* and simulation of *S* at a given time have herein the same weight. After one year of growth, mussel shell length time-series *S(t)* simulated with the Gamma process encompassed the extreme values obtained with the DEB model. At the beginning of the simulations, a higher variability was

Preprints (www.preprints.org) | NOT PEER-REVIEWED | Posted: 16 April 2019 doi:10.20944/preprints201904.0183.v1

Peer-reviewed version available at J. Mar. Sci. Eng. 2019, 7, 158; doi:10.3390/jmse7050158

observed with the Gamma process; this would lead to conservative estimations of marine growth characteristics colonizing the structure. From an engineering purpose, it is essential to reach a good representation of the distribution of maximum values of *S*, which is the case here.

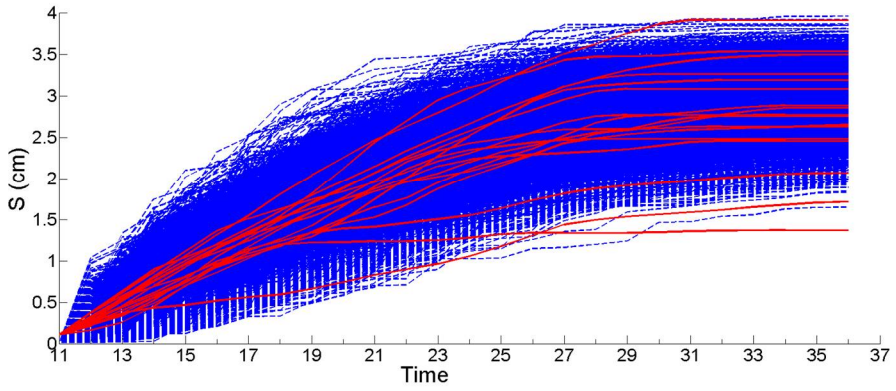

Figure 7. Individual growth trajectories obtained with the DEB model for each year of the 17-year time series (solid red lines) compared with simulated individual growth obtained with the Gamma process approach (dotted blue lines). Time unit represents 10-day periods.

Note that the Gamma process model accounts for stabilization of shell growth during one or several time steps: that phenomenon is observed in the DEB simulation and actually represents a lack of available food. To complete this statistical analysis, the average and the standard deviation of individual shell length curves are presented in Figure 8. They were similar for both methods throughout the simulation period. The Gamma process simulations were a bit conservative in terms of shell length overestimation. The standard deviation curves showed differences between the two approaches. This may be due to the choice of the constant scale parameter β_S, which controls the response dispersion of the Gamma process. Note that there is also a statistical bias when estimating standard deviation from DEB time-series due to the limited amount of data (17 trajectories).

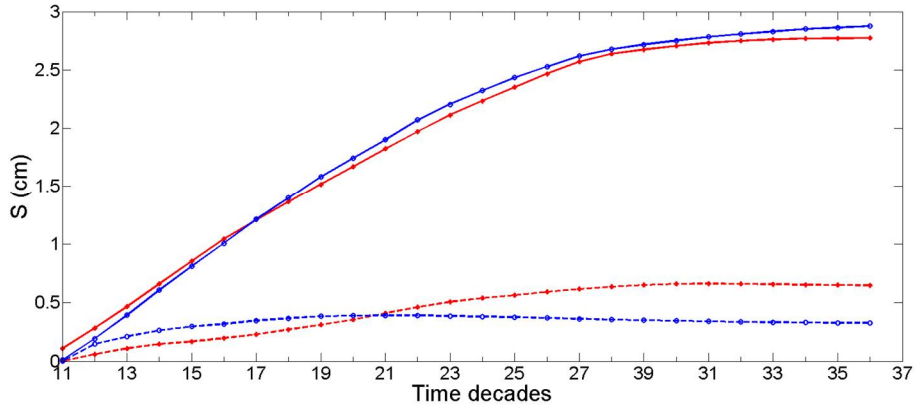

Figure 8. Comparison of average and standard deviation (dashed lines) of shell length from Gamma process (blue lines) and DEB model (red lines). Time unit represents 10-day periods.

2.9 Effect of marine growth and hydrodynamic forces on Jackets

From the structural point of view, marine growth may affect dynamical behavior, resistance to fatigue or extreme loading. We focused here on the latter. Offshore platforms are generally gathered in two families: bottom fixed and floating. Many works studied the effect of marine growth and hydrodynamic forces on components (cylindrical beams) of fixed steel framed offshore structures called jackets for which the component diameter (1 m) is small in comparison with wavelength during storms (100-400 m). This type being, on the one hand, the most popular in oil and gas

industry and also for offshore wind turbines substation, and on the other hand very sensitive to marine growth (fatigue and extreme loading). The analysis of marine growth effect on hydrodynamic forces could be categorized into two groups as follows:

(i) experimental modeling of hydrodynamic forces for cylinders with different roughness conditions ([46]; [47]). Recent studies are mostly concentrated on the water particles velocity and acceleration measurement techniques.

(ii) evaluation of hydrodynamic forces by physical modeling of marine growth characteristics obtained from in-situ measurements ([6]; [48]). These studies were based on inspections carried out during survey campaigns. They advocate guidelines for the probabilistic modeling of hydrodynamic forces at a given time. Biofouling database has been analyzed to propose a model of marine growth evolution and update design criterion. A physical response surface matrix has been proposed in order to provide a probabilistic modeling of the environmental loading on jacket type offshore structures. The key parameter is the increase of structural diameter due to the marine growth thickness.

In the present study, we are considering the non-linear effect of the roughness of marine growth on the loading during a yearly growth. The results from laboratory studies focused mainly (i) on the regular shape of marine growth and homogeneous colonization around the cylinder and (ii) on mean thickness. Moreover, for time computation constraints (stochastic simulations of wave and marine growth) and because it allows introducing explicitly the role of marine growth, we used the Morison modeling [49] for which the link between homogeneous roughness and loading is available. Roughness being non-homogeneous and random in reality, an uncertainty was added.

2.9.1 Effect of marine growth on Morison's equation

Usually, the Morison's model [49] is used to estimate hydrodynamic forces on tubular offshore structures like jackets, using the particle kinematics obtained from the wave heights and periods. It should be noted that for the jacket structures the Morison's equation is valid because the structural diameters (D) are small compared to wavelengths λ ($D/\lambda<0.2$). It can be employed from medium to deep-water depth [49]. It has been shown to be very appropriate for an expansion in the stochastic domain [48]. It is denoted as:

$$F_{Morison} = F_D + F_I = \frac{1}{2}\rho C_D D u|u| + C_m \frac{\rho \pi D^2}{4}\dot{u} \quad (7)$$

Where, F is hydrodynamic force per unit length of the member (N/m), F_D is the drag force per unit length of the member (N/m), F_I is inertia force per unit length of the member (N/m), C_D is the drag coefficient, C_M is inertia coefficient, ϱ is the density of water, D is member diameter (m), u is velocity of wave's water particles (m/s), $\dot{u}$ is the acceleration of wave's water particles (m/s^2). u and $\dot{u}$ are computed by the Stoke's model [50] from the knowledge of metocean data: wave height H and period T.

Generally, the inertia term of the mentioned equation becomes important for small waves or for members with large diameters [48] otherwise the drag term will be dominant. Marine growth increases the surface roughness and hence changes both the drag and inertia forces. Their variations induced by the presence of marine growth, impress the hydrodynamic forces in a non-linear way.

Considering the effect of biofouling on hydrodynamic coefficients in the Morison's equation, some researchers have proposed a model for the drag coefficient as a linear regression function of the thickness and roughness ([51]; ([52]). According to recommended practice of [3], an additional parameter that affects the drag coefficient of elements with circular cross-sections is the relative roughness, $e = k/D_e$. The surface Roughness k is the average peak-to-valley height of hard growth organisms and the effective member diameter De can be obtained as:

$$D_e = D_c + 2\ Th \quad (8)$$

Where D_e is the outer diameter of the clean member and Th is the biocolonization thickness (i.e. the mean of distributed thickness around the diameter) obtained by circumferential measurements [3]. API [3] gives the relationship between De and steady-flow drag coefficient (C_{DS}) (9).

$$C_{DS} = a + \frac{b}{\frac{k}{De} + c};\ a = 0.07152,\ \text{b}=-2.9\times10^{-4},\ \text{c}=4.12\times10^{-4} \quad (9)$$

C_D is then computed from the knowledge of C_{DS} and KC_{mg} according to [3].

This approach allows measuring the influence of roughness on the drag coefficient and therefore the drag force as well as their evolution with time. This brings us to choose an uncertainty modeling for the relationship between the size of the shell and the roughness in Morison's equation.

Coefficients of fluid-structure interactions are modeled from the knowledge of hydraulic flow regime around the structural components [47]. Reynolds R_e and Keulegan-Carpenter KC numbers are essential for characterizing the flow regime [6]. For most offshore jacket structures in the extreme conditions, Reynolds numbers are into the post-critical flow regime, where steady-flow drag coefficient C_{DS} for circular cylinders is independent of Reynolds number [3][53].

2.9.2 Stochastic modeling of marine growth and hydrodynamic parameters

There is not enough knowledge and neither observations about the settlement of blue mussels on offshore structures and a 100% cover was considered on the component. In order to account for the diameter of the colonized structural member, marine growth thickness time-series $Th(t)$ should be modeled. Marine growth thickness is modeled as a Gamma process $Th_{t,\tau}$ deduced from the simulated individual shell length time-series $S_{t,\tau}$ for blue mussels in each time interval. For simplicity and at this step of modeling, it has been assumed that the individual shell length time-series $S(t)$ give the average size time-series $Th_{t,\tau}$ with a multiplying uncertain factor (10): it follows a uniform distribution with support [0.3; 0.6] at each of the i 10-days period.

$$Th(t) = \left\{\left(Th_1,...,Th_n\right);\ 0.3\text{S}_i \le Th_i \le 0.6\text{S}_i, \text{i} \in [\![1,37]\!]\right\} \quad (10)$$

This uncertainty accounts for the geometrical arrangement of the shells (Figure 9).

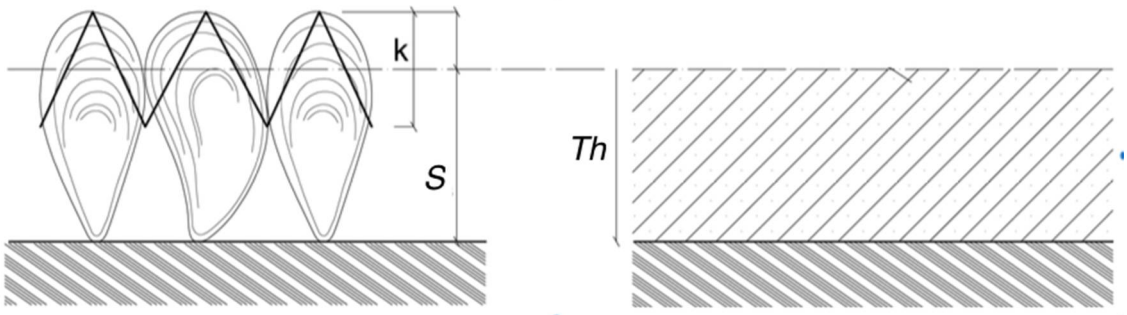

Figure 9. From biological reality to mechanical abstraction.

For roughness, on the one hand, there is a lack of on-site measurements and on the other, the available relationship between roughness and hydrodynamic forces (9) relies on a uniform roughness around the component [3]. Hence, roughness is also modeled as a Gamma process $k_{t,\tau}$ based on individual shell length time-series $S_{t,\tau}$ (11), with a random factor following a uniform distribution with support [0.2; 1]. The latter is a model error for modeling the uncertainty when quantifying the real effect of a randomly distributed roughness around the component. Note that intensive developments on underwater image processing are emerging ([54]-[56]) enabling to

Preprints (www.preprints.org) | NOT PEER-REVIEWED | Posted: 16 April 2019 doi:10.20944/preprints201904.0183.v1

Peer-reviewed version available at J. Mar. Sci. Eng. 2019, 7, 158; doi:10.3390/jmse7050158

envisage progress in on-site measurements and recent works investigate the relationship between non-homogenous roughness and loading ([57]; [58]). The wide range of uncertainty will hence decrease in the next decade. As a consequence, the error of computation of equivalent roughness is significant and the interval in (11) is large: it includes the stochastic distribution of shells around a tubular component and the error of model for computing the equivalent roughness.

Finally, the time-series of surface roughness $k(t)$ and marine growth average thickness $Th(t)$ have been considered independently as the random value uniformly distributed in an interval bounded to a ratio of individual shell length $S(t)$.

$$k(t) = \left\{ \left(k_1, \ldots, k_n \right);\ 0.2\mathrm{S}_n \le \mathrm{k}_n \le \mathrm{S}_n, \mathrm{n} \in [\![1,37]\!] \right\} \quad (11)$$

The relative surface roughness $e(t)$ time-series are deduced ($e(t)= k(t)/De(t)$) and $C_{DS}(t)$ time-series have been simulated according to (9).

This study deals with two major time variant random variables in the hydrodynamic calculations, the meteocean data including a couple of wave height and period (H, T), and the stochastic process generating the individual shell length $S_{t,\tau}$ in each time interval τ from (4). Parameters of Gamma processes $Th_{t,\tau}$, and $k_{t,\tau}$ are dependent of individual shell length St,τ and the hydraulic parameters (Re_{mg}, KC_{mg}), and therefore drag coefficients C_D depend on individual shell length $S_{t,\tau}$ and couple of wave height and period (H, T).

Thus parameters of $Th_{t,\tau}$ affect the hydrodynamic coefficients through the relationships between the hydraulic parameters (R_e, KC) and the diameter of the elements which is dependent of the coefficient of $Th_{t,\tau}$ itself [6]. The next section will explain how these cross-effects are accounted for.

2.9.3 Stochastic modeling wave loading in the presence of marine growth

Figure 10 summarizes the steps of drag forces computation in a flowchart. It should be noted that the steps of hydrodynamic coefficients calculation are based on an interpolation of experimental curves [6] presented by [3].

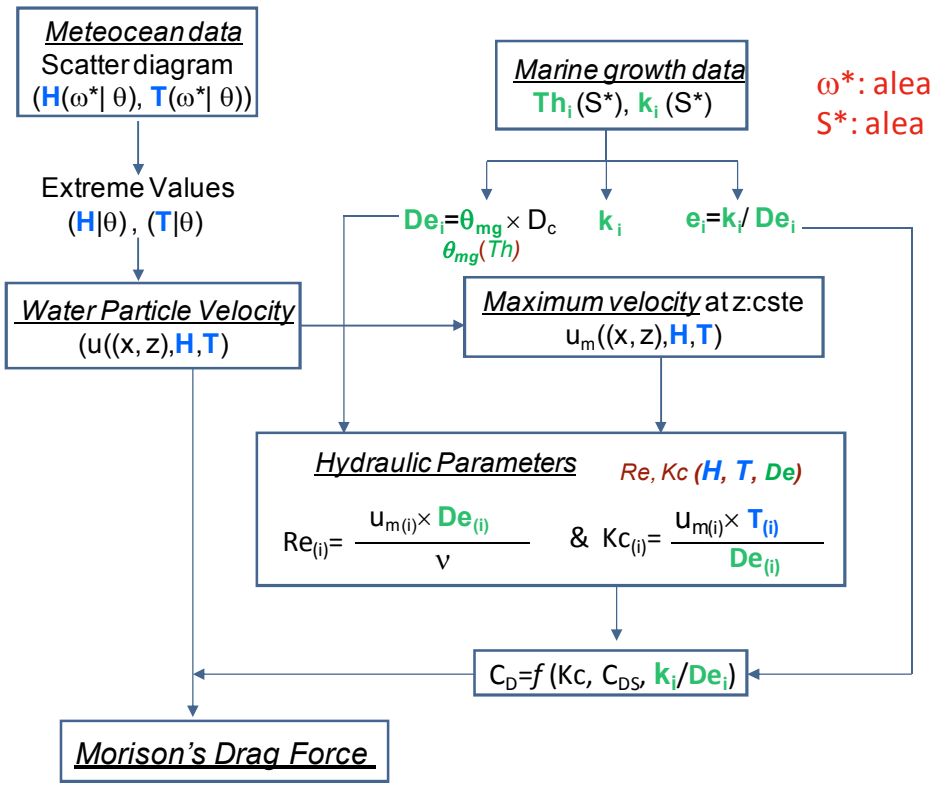

Figure 10. Schematic flowchart of drag force calculation.

Peer-reviewed version available at J. Mar. Sci. Eng. 2019, 7, 158; doi:10.3390/jmse7050158

The main steps of this flowchart are detailed as:

- Statistical Identification: the employed parameters are the heights of extreme waves H and associated periods T. They are modeled with a random variable which probability is conditioned by the wave direction θ;
- A kinematic model for the fluid: the Stokes model [50] is used. It assumes that the fluid is Newtonian and irrotational and the trajectory of fluid particles is elliptical. The kinematics field deduced from the velocity potential can be defined at any point;
- Fluid-structure Interaction model: this level is involved in the hydrodynamic coefficients determined by using the recommendation of [3].
- For the probabilistic modeling of CD, in order to avoid multiplying the case studies, only vertical elements under the wave crest are analyzed. This implies high horizontal speeds and accelerations that generate very small forces; it means that the inertia forces in (7) are very low and will be neglected in the following.
- Colonized diameter De(t) is a stochastic process that results from the increase Th(t) of the initial radius of the clean component. Starting from (8), it is computed by multiplying Dc by factor θmg. The latter is computed from the thickness Th(t) (12):

$$D_e = D_c + 2\,\overline{th} = \theta_{mg}\,D_c \qquad \text{with } \theta_{mg} = \left(1 + \frac{2\,Th_{t,\tau}}{D_c}\right) D_c \tag{12}$$

According to API RP 2A WSD [3] and DNV-RP-C20 [4], since the flow regime is post-critical (R_e>5×105) by using 100 year-return wave characteristics, the drag coefficient does not depend on R_e but rather on KC_{mg} and C_{DS}. Note that API ([3], section C2.3.1b7, p. 143 and p. 145) provides, in fact, a piecewise model on two intervals depending on KC or KC/C_{DS} and the scales of these models are different. It results in two effects on the evolution of the drag force (C_D): first for some values of C_{DS} it is the cause of discontinuity of the model at KC=12 and second, it is very difficult to analyze directly the effect of C_{DS}. This is visible in Figure 15.

Extreme wave characteristics of Gulf of Guinea have been considered for the hydrodynamic calculation; it is a specific site with low KC_{mg} values. Using meteocean data from this region allowed us to cover a large range of KC_{mg} to better illustrate the non-linear effects of marine growth on the drag coefficient evolution and hence on the load probabilistic distribution. Joint distribution of extreme height and period for a return period of 100 years for the Gulf of Guinea are simulated based on [7]. It has been provided by recombination of sea states from the knowledge of *H-T* scatter diagram. Representation of the joint distribution for wave height and period of 100-years return period is presented in [59].

We focused on drag forces acting on vertical cylindrical components under the wave crest with a diameter of 0.762 m (corresponding to the diameter of a Φ30'' leg). Note that the probability of storm occurrence is independent of time and it can happen in every 10-days periods of the macro-colonization period. The time-series of surface roughness *k(t)* and marine growth thickness *Th(t)* obtained from the individual shell length time-series *S(t)* has been considered for determination of C_{DS} (C_D in steady flow) time-series ($C_{DS}(t) = f(kt,\tau\,/D_e)$). In this paper, a numerical fitting of the curve given in [3] is used and is plotted in Figure 15 (lower multi-linear curve for the smooth cylinder).

3. Results

3.1 Simulation of the drag force evolution from the stochastic time-series of blue mussels

This section aims to assess the evolution of the drag coefficient CD by mixing all of the typical macro-colonization time-series according to their occurrence probability by considering the macro-colonization inception times in the initiation phase (section 2.2-2.4). The individual shell length time-series for all of the typical macro-colonization years are necessary to provide the probabilistic matrix of individual shell length. It consists of individual shell length time-series for all

Preprints (www.preprints.org) | NOT PEER-REVIEWED | Posted: 16 April 2019 doi:10.20944/preprints201904.0183.v1

Peer-reviewed version available at J. Mar. Sci. Eng. 2019, 7, 158; doi:10.3390/jmse7050158

typical macro-colonization years. They are weighted by the occurrence probability of each typical macro-colonization year. Therefore, 30,000 simulations (10,000 simulations for each macro-colonization inception time in one year) have been performed to provide the individual shell length of blue mussels for each typical macro-colonization year.

The individual shell length time-series *S(t)* of the blue mussels are simulated from developed Gamma process (section 2.8) from the inception times for typical macro-colonization years. No correlation between macro-colonization inception time conditioned by the temperature and the aggregate *Chl. a* (*Ct*) levels are observed (section 2.6). Therefore, they are simulated independently. Hence, all of the time-series of aggregate *C(t)* could be used for the simulation of individual shell length time-series S(t)) for each typical macro-colonization year.

The individual shell length time-series simulation procedure is as follows: the typical macro-colonization year determined by the temperature is first selected. Then the individual shell length time-series *S(t)* are simulated from the Gamma process. This simulation is performed according to the aggregated *Chl. a* time-series which have been selected randomly, generating one *S(t)* from one *C(t)*. Thus, we obtain the same statistical weight for the inception and growth by choosing an aggregated *Chl. a* time-series randomly for each simulation.

Figure 11 illustrates the estimated individual shell length time-series for the 2nd typical macro-colonization (starting date at 11, 14 and 17 10-day periods) and 200 simulations as an example. The highest jumps are observed for the 18th to 22nd 10-days periods; it is because of the important peak occurrence in the aggregated *Chl. a* time-series in 2001, 2007 and 2008 (see Figure 12).

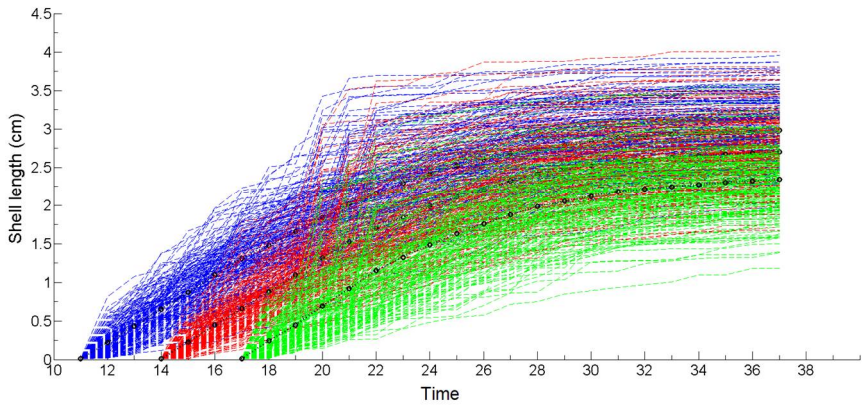

Figure 11. Simulated individual shell length of blue mussels for the 2nd typical macro-colonization. 200 simulations are presented.

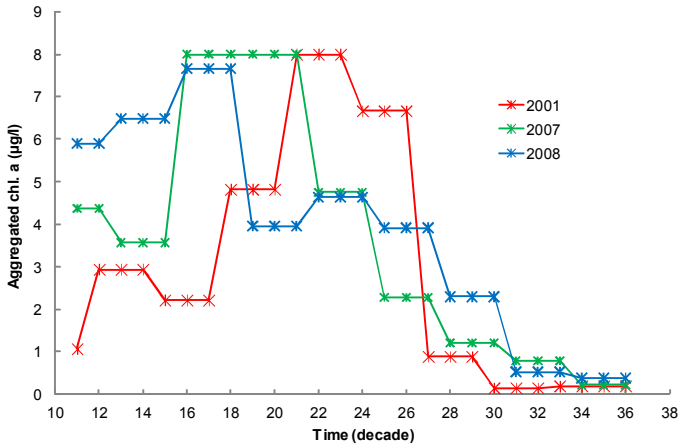

Figure 12. The aggregated *Chl. a* time-series for the years 2001, 2007 and 2008.

Peer-reviewed version available at J. Mar. Sci. Eng. 2019, 7, 158; doi:10.3390/jmse7050158

The simulation allows having the individual shell length matrix representing all of the typical macro-colonization years. The contribution of individual shell length time-series could be obtained as:

$$N_t = N_S \times P_t \quad (13)$$

where, N_t is the numbers of time-series for the typical macro-colonization year of $S(t)$ which should be selected randomly, N_s is the sample size (here equal to 30,000) and P_t is the occurrence probability of the typical macro-colonization year (Table 2). The simulation procedure is illustrated in Figure 13. The KC, C_D and drag forces are then computed according to the flowchart reported in Figure 10.

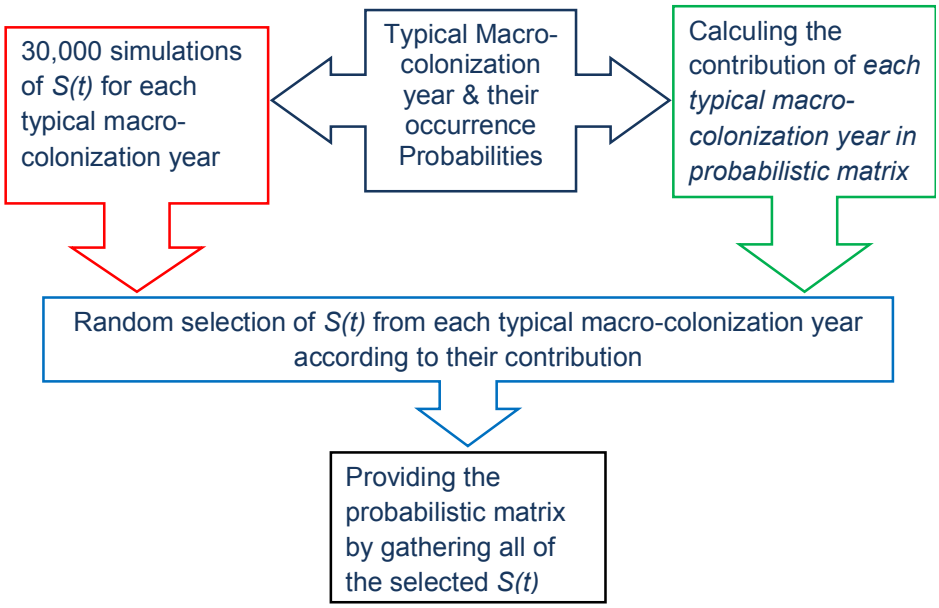

Figure 13. Schematic procedure of probabilistic individual shell length time-series from the typical macro-colonization year.

3.2 *Statistical analysis of the transfer of distributions*

Quality of distribution transfer or uncertainty propagation is a well-known criterion for the analysis of the change of the distribution (its parameters or probabilistic law), especially for matrix response surfaces [48]. We focus first on the evolution of shell length distribution. Figure 14 illustrates the 3 most interesting 10-days periods representing insignificant (11th 10-days period), intermediate (18th 10-days period) and extreme (37th 10-days periods) roughness values. Distribution of shell length changes from bimodal (11th and 18th 10-days period) to normal (37th 10-days periods), depending on time. It should be noted that the shape of the shell length distribution evolves strongly with time; that will lead to significant variations of the distribution of C_D along with its support due to the dependence of C_{DS} to k/D_e in (9). The mixing of sources of uncertainties due to independent macro-colonization inception time and independent growth builds finally a normal distribution as expected from the Central Limit Theorem.

Preprints (www.preprints.org) | NOT PEER-REVIEWED | Posted: 16 April 2019 doi:10.20944/preprints201904.0183.v1

Peer-reviewed version available at J. Mar. Sci. Eng. 2019, 7, 158; doi:10.3390/jmse7050158

632

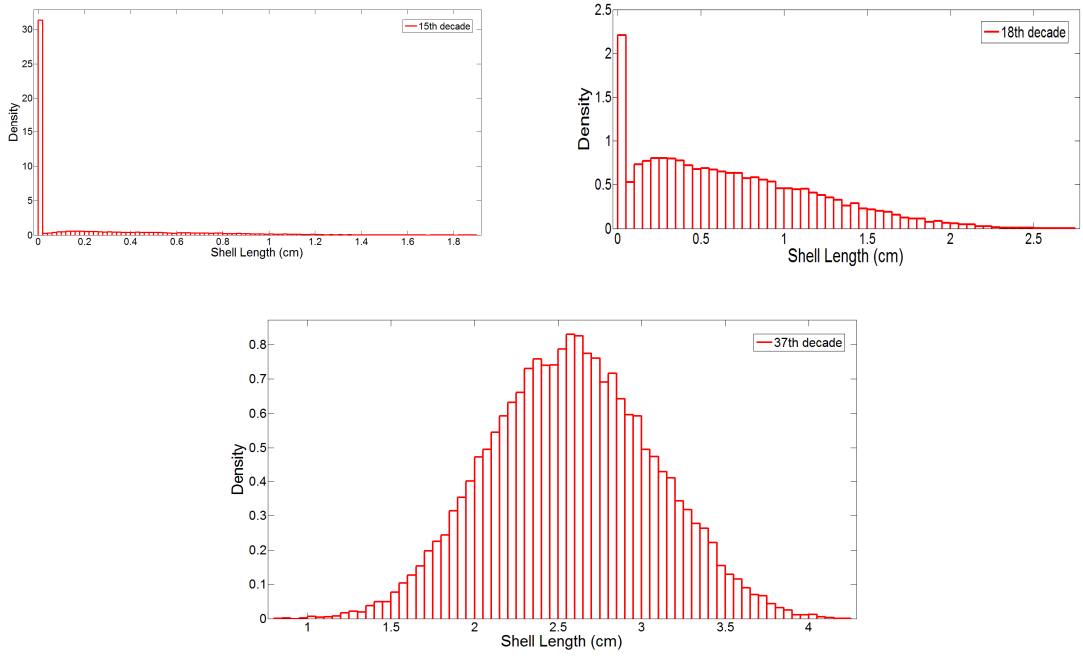

633

634 **Figure 14**. Evolution of shell length distribution as a function of time for three selected 10-days periods. .

635

636 Figure 15 illustrates distributions of drag coefficients C_D as a function of *KC* for the 3
637 above-mentioned 10-days periods. First, we plot the bounds of the relationship (*CD*) - (*KC*) with
638 lower and upper lines that depict respectively the smooth and roughened cylinders drag
639 coefficients. The discontinuity comes from the discontinuity of curves in the standards generated by
640 the various scales (*CD*/*CDS*, *CD*, *KC*, *KC*/*CDS*) used around *KC*=12. Note that this discontinuity for
641 the smooth and roughed cylinders follows respectively a potential positive and a negative jump of
642 the C_D. Second the scatter plots are reported in red, moving from the lower part to the upper part
643 from 11th to 37th decade 10-day periods. Consequently, the distribution of C_D is affected. An
644 important point is that the distribution maintains 2 modes; one, the uppermost being around 1.2 and
645 the lowermost follows the shift of non-linear the transfer function, from 0.2 to 0.6 (see 37th 10-days
646 period). It demonstrates the evolution of the drag coefficients C_D for the individual shell length from
647 the non-linear transfer of the distribution of *KC* and during the probabilistic macro-colonization year
648 (from 11th to 37th 10-days period). Finally, the probability of highest values (typically 1.8) increases
649 with time: that is a key result because it will potentially affect the distribution tail of the
650 corresponding loading and decrease structural reliability. There is not a clear distinction between the
651 macro-colonization inception times because of the mixing of all typical macro-colonization year.
652 Indeed, the mixing of a large amount of potential macro-colonization inception times doesn't allow
653 distinguishing the contribution of each year in terms of the mode in the distribution.

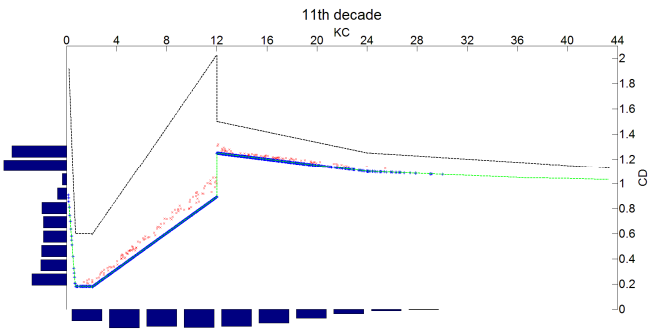

654

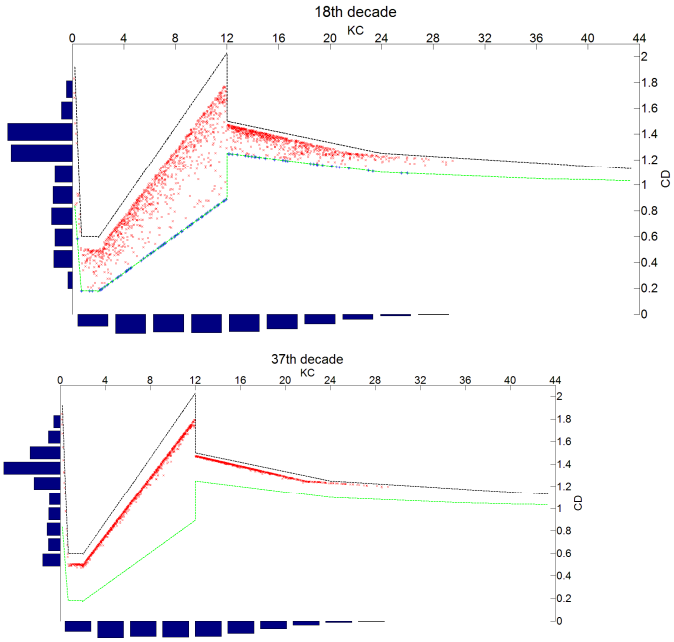

Figure 15. Distributions of drag coefficients (C_D) as a function of (KC) values for three selected time 10-day periods.

4. Discussion

Previous results give the opportunity for discussing the effect of our modeling on post-treated results such as wave loading in presence of marine growth. We compare now the distribution of D_e and C_{DS} (Figure 16). The distributions of D_e are mono-modal because of the combination of all typical macro-colonization years. The distributions of C_{DS} are bimodal and transform to the mono-modal, from the smooth to the ultra-roughened condition at the end of the macro-colonization period.

Distribution of the drag force F_T is plotted on the same figure 16 for better illustrating differences in distribution (mode and tails) and transfer of these distributions. The drag force is exponentially distributed. The right distribution tail moves to higher values according to time, decreasing the reliability. We analyze this distribution tail after computation of F_{T_MAX} (note that distributions are bounded) and the fractiles $F_{T(90\%)}$, $F_{T(95\%)}$. Figure 17 shows the evolution of these statistics after each 10-days period. The latter increase smoothly with time except for the increase during one month and a half (from 10-days period 11th to 18th). Finally, there is a great difference between the extreme values (F_{T_MAX}) and the fractiles ($F_{T(90\%)}$ and $F_{T(95\%)}$ confirming a long distribution tail that was observed already on Figure 16.

Preprints (www.preprints.org) | NOT PEER-REVIEWED | Posted: 16 April 2019 doi:10.20944/preprints201904.0183.v1

Peer-reviewed version available at J. Mar. Sci. Eng. 2019, 7, 158; doi:10.3390/jmse7050158

674

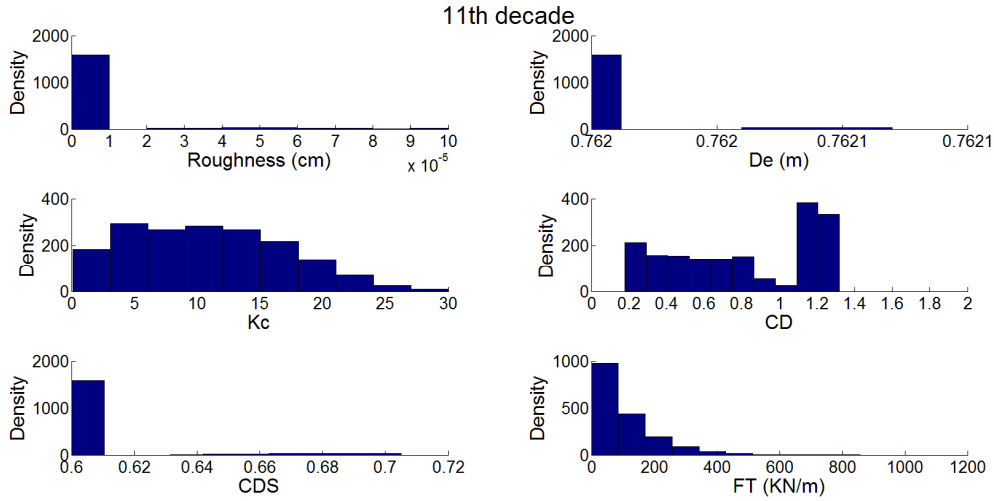

675

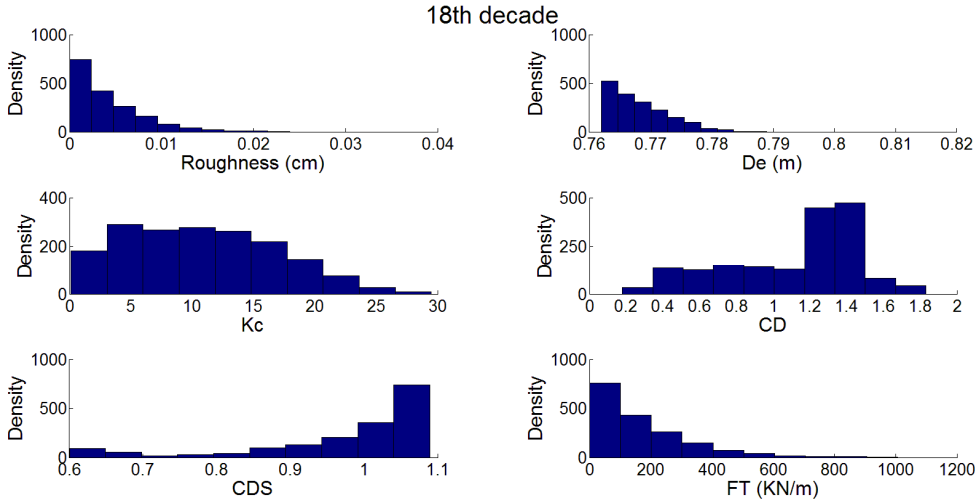

676

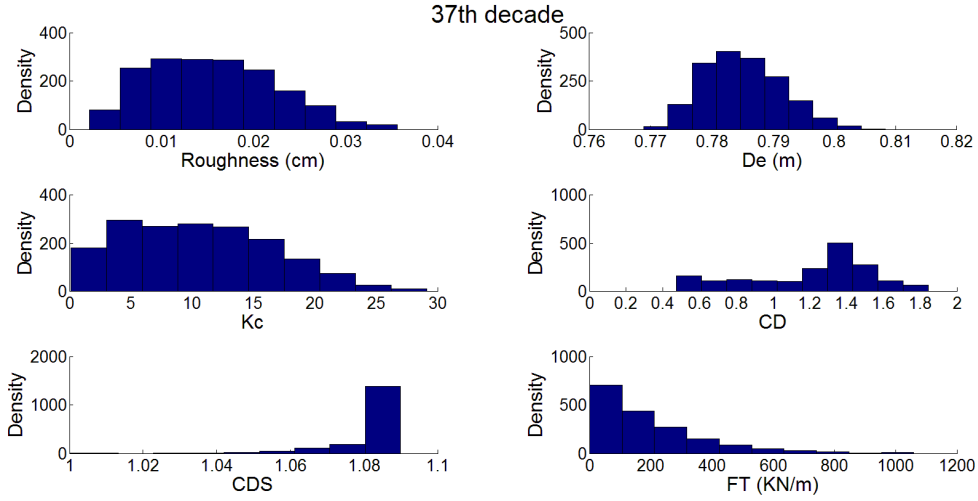

677
678

679 **Figure 16**. Comparison of the distribution of hydrodynamic parameters for selected 10-days periods. .

680

Preprints (www.preprints.org) | NOT PEER-REVIEWED | Posted: 16 April 2019 doi:10.20944/preprints201904.0183.v1

Peer-reviewed version available at J. Mar. Sci. Eng. 2019, 7, 158; doi:10.3390/jmse7050158

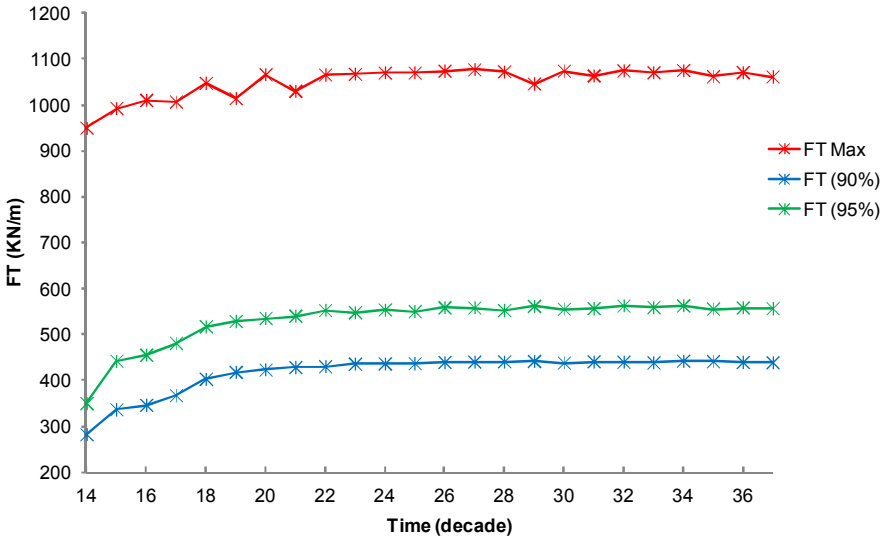

Figure 17. Evolution of F_{Tmax}, and 90%, 95% fractiles with time. .

5. Conclusions

The originality of this work lies in the choice to consider biocolonization as a cumulative deterioration phenomenon and to simulate trajectories relying on individuals' characteristics through a state-dependent model to compute structural reliability. The developed non-stationary, state-dependent Gamma process was selected as a flexible methodology and simple to perform. It was used to generate individual shell length time-series for blue mussels. The macro-colonization inception times determined in the initiation phase may be considered as one of the criteria for the installation or cleaning time of the structures through the maintenance programs strategy. One of its advantages is that it can be extended to other organisms such as oysters with the possibility of adding or modifying the parameters influencing individual growth and shape.

A model was used to investigate the drag coefficient evolution exerted by extreme waves during the mussel's growth. Three types of uncertainties have thus been considered:

- Environmental: due both to the physics of waves (height, period) and water parameters (temperature and chlorophyll a),
- Modeling: with an uncertainty of modeling from the shell size to the thickness and the roughness in the sense of API regulation,
- Biological: accounting for the inter-individual variability.
- Moreover, calculation of hydrodynamic forces due to the biocolonization using meteo-ocean data as well as biological data is a complex task and generates two types of difficulties:
- The distribution of input variables that can be pluri-modal (e.g. individual shell length) due to the various macro-colonization inception times;
- The transfer from Keulegan Carpenter number to drag coefficient being nonlinear generates bimodal distributions from mono-modal ones.

A full probabilistic simulation that allows predicting the evolution of drag forces in a reliability context has been developed. The evolution of physical parameters due to the individual growth has been presented in time-series form. Using the empirical curves recommended by API standards to obtain wake amplification factors in a probabilistic context resulted in an abnormal discontinuity when passing the critical value KC=12. Hence these curves may not perfectly explain the evolution of drag coefficient in a probabilistic context.

This study highlights the site-specific property of biofouling and therefore, constructs a condition-based methodology for the modeling of biocolonization. Considering the site-specific property of biofouling, it is not logical to define a similar strategy for the maintenance and periodical cleaning programs of offshore structures without consideration of the specifications of each site.

Peer-reviewed version available at J. Mar. Sci. Eng. 2019, 7, 158; doi:10.3390/jmse7050158

Therefore, periodical monitoring campaigns could be very useful in understanding the reaction of biofouling to environmental parameters, especially after installation or cleaning programs, and to establishing the adequate maintenance strategy for each site. It allows the model to be updated as well and hence increases the prediction accuracy. For some structures, it may not be necessary to clean all members completely to allow a macro-fouling community to develop and create artificial reefs that would be useful for fisheries and biodiversity. This work can be extended to floating structure once the correlation between thickness and weight is known.

6. Patents

A patent was developed in view to measure on site the marine growth and update the model: Schoefs F., Ameryoun H. (2013) « Biocolmar: Offshore Station for Measuring and Collecting Data in an Underwater Environment », october 21th 2013, N° 1360256.

Author Contributions: F. Schoefs: methodology for coupling the models and developing gamma processes – stochastic computation; H. Ameryoun: methodology numerical implementation; L. Barillé: environmental modeling and metabolism of mussels; Y. Thomas: simulation of MEB model.$

Acknowledgments: The authors acknowledge the Sea and Littoral Research Institute (www.iuml.fr) for supporting the initiation of work and Région Pays de la Loire to give the opportunity to deepen it in COSELMAR (2012-2016) an SI3M (2008-2012) projects.

Appendix A

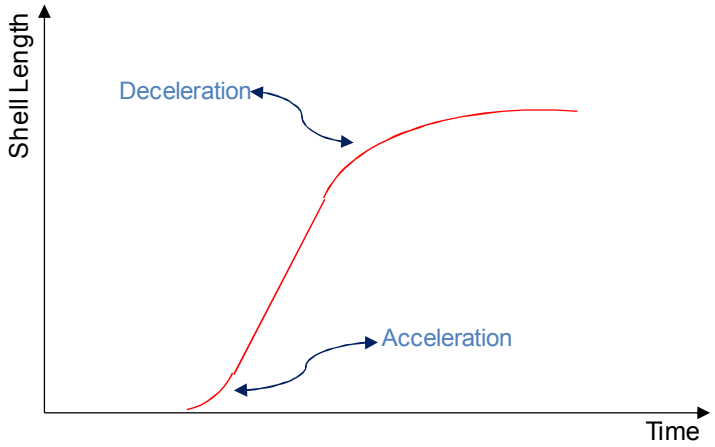

Figure A1. Schematic annual growth curve of individual blue mussels illustrating the acceleration and deceleration in the growth rate. .

Preprints (www.preprints.org) | NOT PEER-REVIEWED | Posted: 16 April 2019 doi:10.20944/preprints201904.0183.v1

Peer-reviewed version available at J. Mar. Sci. Eng. 2019, 7, 158; doi:10.3390/jmse7050158

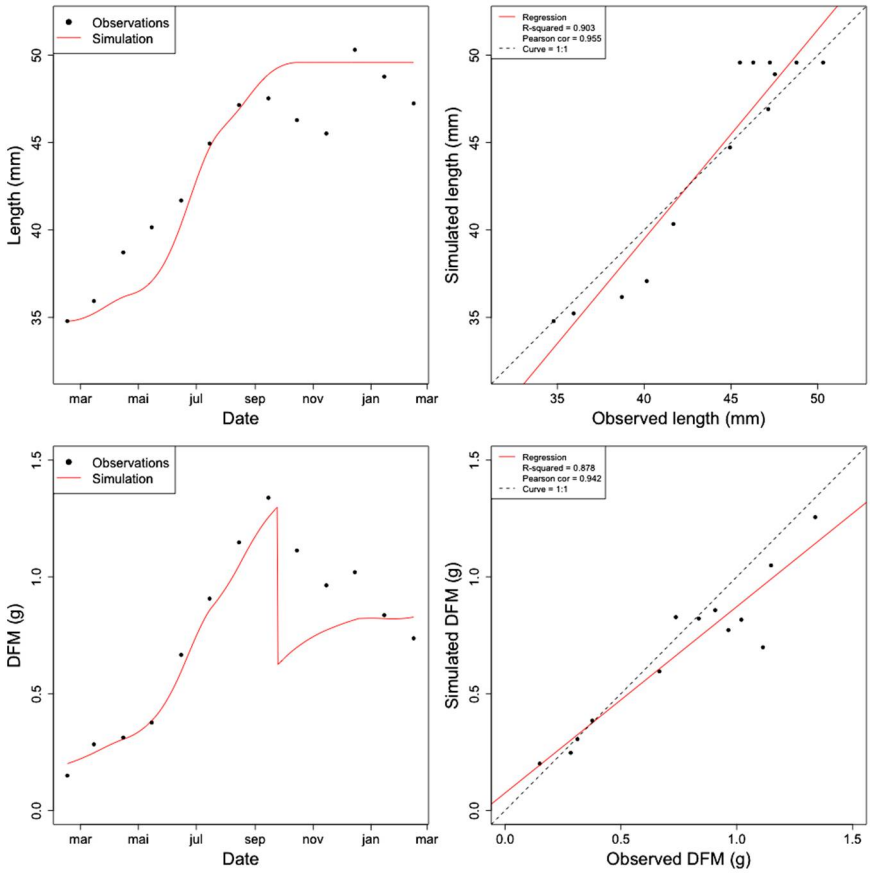

Figure A2. Calibration of the mussel DEB model used in this study to simulate shell length. DFM =Dry Flesh Mass expressed in g.

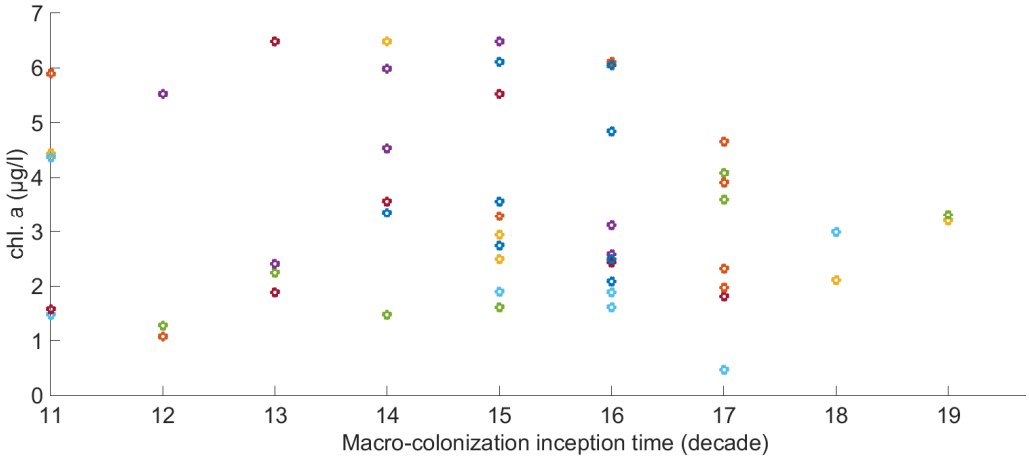

Figure A3. The relationship between macro-colonization starting times (end of the initiation phase) expressed in 10-days; each color represents a year of the 1996-2012 time-series.

References

1. Heaf, N. J. The Effect Of Marine Growth On The Performance Of Fixed Offshore Platforms In The North Sea. In M. F. of O. Platforms (Ed.), *Offshore Technology Conference*, **1979**, (p. 14). Houston: Offshore Technology Conference. http://doi.org/10.4043/3386-MS.

2. Jusoh, I., & Wolfram, J. Effects of marine growth and hydrodynamic loading on offshore structures. *Journal Mekanikal*, **1996**, 77–98.
3. API RP 2A WSD. Recommended practice for planning, designing, and constructing fixed offshore platforms (21st ed., Vol. 2). **2005**, Washington.
4. DNV-RP-C20. Recommended Practice Det Norske Veritas. Dnv. **2010** (DNV-RP-C20).
5. Faber, M. H., Hansen, P. F., Jepsen, F. D., & Moller, H. H. Reliability-Based Management of Marine Fouling. *Journal of Offshore Mechanics and Arctic Engineering*, **2001**, 123(2), 76. http://doi.org/10.1115/1.1355773.
6. Schoefs, F., & Boukinda, M. L. Sensitivity Approach for Modeling Stochastic Field of Keulegan–Carpenter and Reynolds Numbers Through a Matrix Response Surface. *Journal of Offshore Mechanics and Arctic Engineering*, **2010**, 132(1), 011602. http://doi.org/10.1115/1.3160386.
7. Boukinda, M. L. Surface de réponse des efforts de houle des structures jackets colonisées par des bio-salissures. **2007**, PhD Thesis. Nantes.
8. Schoefs, F., & Boukinda, M. L. Modelling of Marine Growth Effect on Offshore Structures Loading Using Kinematics Field of Water Particle, In *ISOPE Proc.*, **2004**, (pp. 419–427). Toulon.
9. Joschko, T. J., Buck, B. H., Gutow, L., & Schröder, A. Colonization of an artificial hard substrate by Mytilus edulis in the German Bight. *Marine Biology Research*, **2008**, 4(5), 350–360. http://doi.org/10.1080/17451000801947043.
10. Maar, M., Bolding, K., Petersen, J. K., Hansen, J. L. S., & Timmermann, K. Local effects of blue mussels around turbine foundations in an ecosystem model of Nysted off-shore wind farm, Denmark. *Journal of Sea Research*, **2009**, 62(2–3), 159–174. http://doi.org/10.1016/j.seares.2009.01.008
11. Koojiman, S. *Dynamic Energy and Mass Budgets in Biological Systems*. **2000**, Cambridge University Press.
12. Koojiman, S. *Dynamic Energy Budget theory for metabolic organisation*. **2000**, Cambridge University Press.
13. El Hajj, B., Schoefs, F., Castanier, B., & Yeung, T. A condition-based deterioration model for the stochastic dependency of corrosion rate and crack propagation in a submerged concrete structure. *Computer Aided Civil and Infrastructure Engineering*, **2014**, 103(4).
14. Ameryoun, H. Probabilistic Modeling of Wave Actions on Jacket Type Offshore Wind Turbines in Presence of Marine Growth. **2015**. PhD Thesis. Université de Nantes.
15. Dürr, S., & Thomason, J. *Biofouling*. New York: Wiley-Blackwell. **2009**, Retrieved from http://eu.wiley.com/WileyCDA/WileyTitle/productCd-1405169265.html.
16. Railkin, A. I. *Marine Biofouling*: Colonization Processes and Defenses. **2003**, CRC Press.
17. Liu, Y. Modeling the Time-to-Corrosion Cracking of the Cover Concrete in Chloride Contaminated Reinforced Concrete Structures. **1996**. PhD Thesis. Virginia Polytechnic Institute and State University.
18. Newell, R. I. E. Species Profiles : Life Histories and Environmental Requirements of Coastal Fishes and Invertebrates (North and Mid-Atlantic). *Biological Report*, **1989**, 82(11.102) TR EL-82-4 June 1989
19. Bruijs, M. C. M. Biological Fouling Survey of marine fouling on turbine support structures of the Offshore Windfarm Egmond aan Zee. Report prepared for Noordzeewind. **2010**, 50863511-TOS/PCW 10-4207, OWEZ_R_112_T1_20100226, KEMA Nederland B.V., Arnhem, the Netherlands..
20. Langhamer, O., Wilhelmsson, D., & Engström, J. Artificial reef effect and fouling impacts on offshore wave power foundations and buoys – a pilot study. Estuarine, *Coastal and Shelf Science*, **2009**, 82(3), 426–432. http://doi.org/10.1016/j.ecss.2009.02.009.
21. Gosling, E. Bivalve Molluscs: Biology , Ecology and Culture. **2003**, Oxford: Wiley-Blackwel.
22. Barillé Boyer, A.-L. Contribution à l'étude des potentialités conchylicoles du Pertuis Breton. **1996**. PhD Thesis. Université d'Aix-Marseille II.
23. Garen, P., Robert, S., & Bougrier, S. Comparison of growth of mussel, Mytilus edulis, on longline, pole and bottom culture sites in the Pertuis Breton, France. *Aquaculture*, **2004**, 232(1–4), 511–524.
24. Rosland, R., Strand, Ø., Alunno-bruscia, M., Bacher, C., & Strohmeier, T. Applying Dynamic Energy Budget (DEB) theory to simulate growth and bio-energetics of blue mussels under low seston conditions. *Journal of Sea Research*, **2009**, 62(2–3), 49–61.
25. Widdows, J. Physiological ecology of mussel larvae. *Aquaculture*, **1991**, 94(2–3), 147–163. http://doi.org/10.1016/0044-8486(91)90115-N.
26. Dutertre, M., Beninger, P. G., Barillé, L., Papin, M., Rosa, P., Barillé, A-L., & Haure, J. Temperature and seston quantity and quality effects on field reproduction of farmed oysters, Crassostrea gigas , in Bourgneuf Bay, France. *Aquatic Living Resources*, **2009**, 22(3), 319–329. http://doi.org/10.1051/alr/2009042

27. Bayne, B. L. Growth and the delay of metamorphosis of the larvae of Mytilus edulis (L.). *Ophelia*, **1965**, 2(1), 1–47. http://doi.org/10.1080/00785326.1965.10409596.
28. Bayne, B. L., & Worrall, C. M. Growth and Production of Mussels Mytilus edulis from Two Populations. *Marine Ecology*, **1980**, 3, 317–328.
29. Van Harden, R., & Koojiman, S. Application of a Dynamic Energy Budget Model to Mytilus Edulis (L.). *Netherlands Journal of Sea Research*, **1993**, 31(2), 119–133.
30. Page, H.M., H. D. M. Temporal and spatial patterns of growth in mussels Mytihs edulis on an offshore platform : relationships to water temperature and food availability. *Experimental Marine Biology and Ecology*, **1987**, 111, 159–179.
31. Thomas, Y., Mazurié, J., Alunno-Bruscia, M., Bacher, C., Bouget, J.-F., Gohin, F., Pouvreau S. & Struski, C. Modelling spatio-temporal variability of Mytilus edulis (L.) growth by forcing a dynamic energy budget model with satellite-derived environmental data. *Journal of Sea Research*, **2011**, 66(4), 308–317.
32. Thompson, R. Production, reproductive effort, reproductive value and reproductive cost in a population of the blue mussel Mytilus edulis from a subarctic environment. *Marine Ecology Progress Series*, **1984**, 16, 249–257. http://doi.org/10.3354/meps016249
33. Hernández Fariñas, T. H. F. Analyse et modélisation des évolutions à long terme de la biodiversité phytoplanctonique dans les zones côtières sous l'effet des pressions environnementales et anthropiques. **2015**, PhD. Thesis. Université de Nantes.
34. Hernandez-Farinas, T., Soudant, D., Barille, L., Belin, C., Lefebvre, A., & Bacher, C. Temporal changes in the phytoplankton community along the French coast of the eastern English Channel and the southern Bight of the North Sea. *Marine Science*, **2013**, 70, 1439–1450.
35. Barillé, L., Lerouxel, A., Dutertre, M., Haure, J., Barillé, A. L., Pouvreau, S., & Alunno-Bruscia, M. Growth of the Pacific oyster (Crassostrea gigas) in a high-turbidity environment: Comparison of model simulations based on scope for growth and dynamic energy budgets. *Journal of Sea Research*, **2011**, 66(4), 392–402. http://doi.org/10.1016/j.seares.2011.07.004
36. Handå, A., Alver, M., Edvardsen, C. V., Halstensen, S., Olsen, A. J., Øie, G., … Reinertsen, H. Growth of farmed blue mussels (Mytilus edulis L.) in a Norwegian coastal area; comparison of food proxies by DEB modeling. *Journal of Sea Research*, **2011**, 66(4), 297–307.
37. Pouvreau, S., Bourles, Y., Lefebvre, S., Gangnery, A., & Alunno-Bruscia, M. Application of a dynamic energy budget model to the Pacific oyster, Crassostrea gigas, reared under various environmental conditions. *Journal of Sea Research*, **2006**, 56(2), 156–167. http://doi.org/10.1016/j.seares.2006.03.007
38. Ren, J. S., & Ross, A. H. Environmental influence on mussel growth: A dynamic energy budget model and its application to the greenshell mussel Perna canaliculus. *Ecological Modelling*, **2005**, 189(3–4), 347–362.
39. Barillé, L., Prou, J., Héral, M., & Razet, D. Effects of high natural seston concentrations on the feeding, selection, and absorption of the oyster Crassostrea gigas (Thunberg). *Journal of Experimental Marine Biology and Ecology*, **1997**, 212(2), 149–172. http://doi.org/10.1016/S0022-0981(96)02756-6
40. Bayne, B. L., & Newell, R. C. Physiological energetics of marine molluscs. *The Mollusca*, **1983**, 4, 407–515.
41. Van Noortwijk, J. M. A survey of the application of gamma processes in maintenance. *Reliability Engineering & System Safety*, **2009**, 94(1), 2–21.
42. Abdel-Hameed, M. A Gamma Wear Process. *IEEE Transactions on Reliability*, **1975**, R-24(JUNE), 152–153. http://doi.org/10.1109/TR.1975.5215123.
43. Cheng, T., Pandey, M. D., & Van Der Weide, J. a M. (2012). The probability distribution of maintenance cost of a system affected by the gamma process of degradation: Finite time solution. Reliability Engineering and System Safety, 108, 65–76. http://doi.org/10.1016/j.ress.2012.06.005.
44. Van Noortwijk, J. M., Van der Weide, J. a M., Kallen, M. J., & Pandey, M. D. Gamma processes and peaks-over-threshold distributions for time-dependent reliability. *Reliability Engineering and System Safety*, **2007**, 92, 1651–1658. http://doi.org/10.1016/j.ress.2006.11.003.
45. Guida, M., Postiglione, F., & Pulcini, G. A time-discrete extended gamma process for time-dependent degradation phenomena. *Reliability Engineering and System Safety*, **2012**, 105, 73–79. http://doi.org/10.1016/j.ress.2011.12.016.
46. Sarpkaya, T. On the Effect of Roughness on Cylinders. *Journal of Offshore Mechanics and Arctic Engineering*, **1990**, 112(4), 334. http://doi.org/10.1115/1.2919875.
47. Theophanatos, A. Marine growth and the hydrodynamic loading of offshore structures. **1988**, PhD Thesis, University of Srathclyde.

857 48. Schoefs, F. Sensitivity approach for modelling the environmental loading of marine structures through a
858 matrix response surface. *Reliability Engineering & System Safety*, **2008**, 93(7), 1004–1017.
859 http://doi.org/10.1016/j.ress.2007.05.006.
860 49. Morison, J. R., Johnson, J. W., & Schaaf, S. A. The Force Exerted by Surface Waves on Piles. *Journal of*
861 *Petroleum Technology*, **1950**, 2(05), 149–154. http://doi.org/10.2118/950149-G.
862 50. Stokes, G. G. On the theory of oscillatory waves. *Trans. Camb. Phil. Soc.*, **1847**, 8, 441–455.
863 51. Wolfram, J., Jusoh, I., & Sell, D. Uncertainty in the Estimation of Fluid Loading Due to the Effects of
864 Marine Growth, *Safety and Reliability Symposium, Proc. of 12th int. conf. on Offshore Mechanics and Arctic*
865 *Engineering*, **1993**, vol. II, pp. 219–228, O.M.A.E'93, Glasgow.
866 52. Kasahara, Y., Koterayama, W., & Shimazaki, K. Wave Forces Acting on Rough Circular Cylinders at High
867 Reynolds Numbers. In *Offshore Technology Conference*, **2013**, p. 12). Houston,
868 http://doi.org/10.4043/5372-MS.
869 53. Troesch, a. W., & Kim, S. K. Hydrodynamic forces acting on cylinders oscillating at small amplitudes.
870 *Journal of Fluids and Structures*, **1991**, 5, 113–126. http://doi.org/10.1016/0889-9746(91)80014-5.
871 54. O'Byrne, M., Schoefs, F., Pakrashi, V. & Ghosh, B.. An underwater lighting and turbidity image repository
872 for analysing the performance of image based non-destructive techniques. *Structure and Infrastructure*
873 *Engineering - Maintenance, Management, Life-Cycle Design and Performance*. **2018**, 14:1, 104-123,
874 doi:10.1080/15732479.2017.1330890.
875 55. O'Byrne, M., Schoefs, F., Pakrashi, V. & Ghosh, B. A Stereo-Matching Technique for Recovering 3D
876 Information from Underwater Inspection Imagery. *Computer Aided Civil And Infrastructure Engineering*,
877 **2018**, 33(3), 193–208, doi.org/ 10.1111/mice.12307.
878 56. O'Byrne, M., Pakrashi, V., Schoefs, F. & Ghosh B. Semantic Segmentation of Underwater Imagery Using
879 Deep Networks. *Journal of Marine Science and Engineering - section: Ocean Engineering*. **2018**. Special Issue
880 "Underwater Imaging", 6: 93.
881 57. Zeinoddini, M., Bakhtiari, A., Schoefs, F. & Zandi A. P. (2017). Towards an Understanding of the Marine
882 Fouling Effects on VIV of Circular Cylinders: Partial Coverage Issue. Biofouling. 33:3, 268-280, doi:
883 10.1080/08927014.2017.1291803.
884 58. Bakhtiari, A., Schoefs, F. & Ameryoun, H. Unified Approach For Estimating Of The Drag Coefficient In
885 Offshore Structures In Presence Of Bio-Colonization. *Proc. of 37th int. conf. on Offshore Mechanics and Arctic*
886 *Engineering*, **2018**, (O.M.A.E'18), paper 78757, June 17-22, 2018, Madrid, Spain.
887 59. Nerzic, R., Prevosto, M., Frelin, C., & Quiniou, V. Joint Distributions for Wind/waves/current in West
888 Africa and derivation of Multi Variate Extreme I-FORM Contours. *In 17th International Offshore and Polar*
889 *Engineering Conference*, **2007**, pp. 81–88, Lisbon: ISOPE.
890

891